Available online at www.sciencedirect.com
ScienceDirect
Quaternary Geochronology 3 (2008) 213–225
QUATERNARY GEOCHRONOLOGY
www.elsevier.com/locate/quageo

Mid-Holocene variability in the marine ^{14}C reservoir age for northern coastal Papua New Guinea

H.V. McGregor[a,b,c,*], M.K. Gagan[a], M.T. McCulloch[a], E. Hodge[b], G. Mortimer[a]

[a]*Research School of Earth Sciences, The Australian National University, Canberra, ACT 0200, Australia*
[b]*Institute for Environmental Research, Australian Nuclear Science and Technology Organisation, PMB1, Menai, NSW 2234, Australia*
[c]*School of Earth and Environmental Sciences, University of Wollongong, NSW 2522, Australia*

Received 17 April 2007; received in revised form 13 November 2007; accepted 18 November 2007
Available online 23 November 2007

Abstract

Changes in oceanic radiocarbon (^{14}C) reservoir ages through the deglaciation and Holocene can provide important information on ocean circulation as Earth's climate warmed. Here, we present reservoir ages for the western tropical Pacific that span the mid-Holocene transition from less to more frequent El Niño events. Reservoir ages were calculated using paired U–Th and conventional ^{14}C dating of eight individual fossil coral samples from Koil and Muschu Islands, northern coastal Papua New Guinea (PNG). AMS ^{14}C and MC-ICPMS U–Th dating of additional samples from six of the fossil corals were used to confirm the TIMS U–Th and conventional ^{14}C ages. The combined results show average reservoir ages of 185 ± 30 ^{14}C yr ($n = 4$) for 7220–5850 yr BP compared to 420 ^{14}C yr for a modern coral from Muschu Island. From 5850 to 5420 yr BP reservoir ages increase to modern values. The relatively young reservoir ages from 7220 to 5850 yr BP are best explained by greater influx of well-equilibrated sub-tropical water from the southern branch of the South Equatorial Current (SEC). This is consistent with strengthening trade winds (facilitating air–sea exchange) and a more northerly position of the Intertropical Convergence Zone thought to have occurred at this time. The transition to more modern-like reservoir ages from 5850 to 5420 yr BP suggests modern oceanic circulation patterns were established during this interval. The onset of modern El Niño activity around this time would have served to enhance the intrusion of ^{14}C-depleted equatorial waters via the south equatorial branch of the SEC. Overall, the changes in reservoir age presented here for the western tropical Pacific suggest that Holocene changes in the El Niño–Southern Oscillation state of the tropical Pacific resulted in reorganisation of oceanic circulation in this region.

Keywords: Radiocarbon; Reservoir age; ΔR; U–Th dating; Holocene; Western Pacific warm pool; Coral; ENSO

1. Introduction

Radiocarbon ages of marine fossil samples must be corrected for differences between the radiocarbon age of surface water and the contemporaneous atmosphere prior to calculation of a calendar age. This is because the waters of the deep ocean are out of equilibrium with respect to the atmosphere causing marine carbon-containing material to appear older than material formed at the same time on land (in equilibrium with the atmosphere). The difference in radiocarbon "age" of the global surface ocean compared to the atmosphere ^{14}C is termed the global marine reservoir age ($R(t)$, Stuiver and Polach, 1977).

When converting marine radiocarbon ages to calendar ages, the global marine reservoir age is taken into account if the Marine04 curve is used for the calibration (Hughen et al., 2004). For the Holocene period, the Marine04 curve $R(t)$ was modelled to vary with time due to changes in the atmospheric ^{14}C production rate (Hughen et al., 2004).

In addition to production rate changes there may also be local differences in the reservoir age (R) due to ocean–atmosphere exchange, ocean ventilation (upwelling), and thermohaline circulation (Adkins et al., 1998; Sikes et al., 2000; Siani et al., 2001; Fontugne et al., 2004). For example, increased upwelling brings "older" water to the

*Corresponding author at: School of Earth and Environmental Sciences, University of Wollongong, NSW 2522, Australia.
Tel.: +61 2 4221 4265; fax: +61 2 4221 4250.
E-mail address: mcgregor@uni-bremen.de (H.V. McGregor).

1871-1014/$ - see front matter
doi:10.1016/j.quageo.2007.11.002

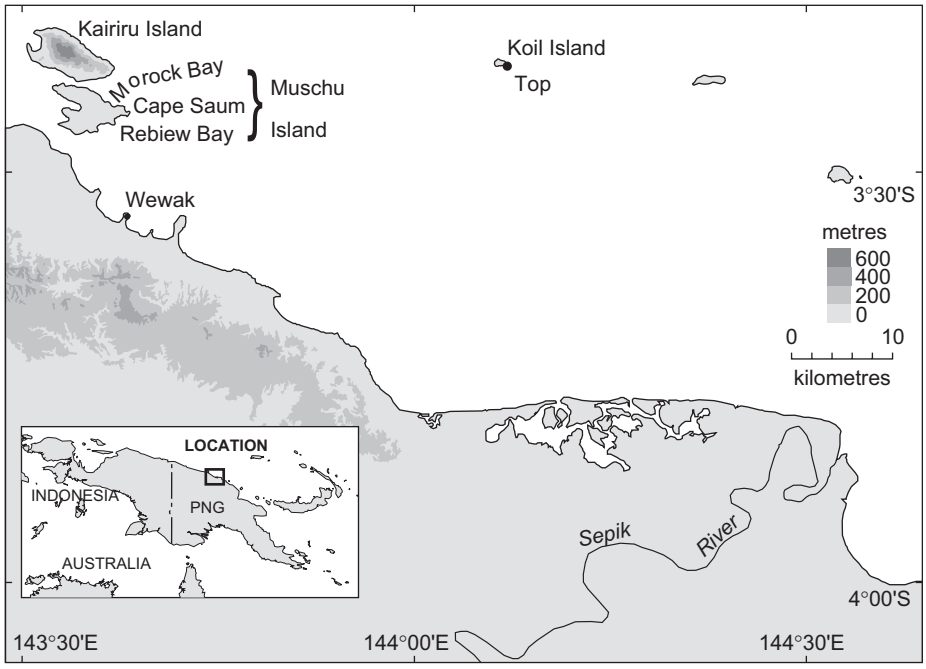

Fig. 1. Physiographic map showing fossil coral sampling locations: Rebiew Bay and Morock Bay, Muschu Island and Top Point Breach, Koil Island. The modern coral used to calculate the modern ΔR and reservoir age was collected from a fringing reef at Cape Saum, Muschu Island.

surface, making reservoir ages greater. The difference between local R and that for the Marine04 curve, termed ΔR, must be subtracted prior to calibration of marine radiocarbon dates. ΔR in modern samples is known to vary spatially (Reimer and Reimer, 2001); however, it is assumed to be constant through time for any given marine location (Hughen et al., 2004).

Here, we explore reservoir age variability in the little-studied tropical western Pacific Ocean and test the assumption of constant ΔR through the mid- to late Holocene for the northern coast of Papua New Guinea (PNG). Reservoir ages were calculated using paired radiocarbon and U–Th dating on eight fossil corals from Muschu and Koil Islands, PNG (Fig. 1), a site known to be sensitive to El Niño–Southern Oscillation variability (McGregor and Gagan, 2004). The results show a marked reduction in reservoir age for the mid-Holocene and suggest the influence of well-equilibrated waters of the South Equatorial Current (SEC) at the site, consistent with a greater tendency to La Niña-like conditions during the early to mid-Holocene.

2. Oceanographic setting

Koil Island (03°21′S, 144°08′E), part of the Schouten Island Group, is located 73 km northwest of the Sepik River mouth and Muschu Island (03°25′S, 143°35′E) 115 km west of the Sepik River mouth (Fig. 1). The Muschu and Koil Island region is characterised by high rainfall with average annual rainfall at nearby Wewak of 2000 mm/yr (McAlpine et al., 1983). In general, northwest winds prevail from November to March (NW monsoon), and southeast winds dominate from May to August (SE monsoon) (McAlpine et al., 1983).

Koil and Muschu Islands are in the heart of the oceanic water mass known as the Western Pacific Warm Pool (WPWP). This is the warmest body of ocean water in the world and is located in the Indo-Pacific region. It has an average annual sea surface temperature (SST) of $>28\,^{\circ}C$ (Yan et al., 1992; Levitus and Boyer, 1994), and has also been termed the "fresh pool" due to its relatively low salinity (<35 psu, Hénin et al., 1998). Mean winds are low and convergence of moist air is at a maximum in this region (Tourre and White, 1997). Small changes in SST (0.5–1 °C) in the WPWP can result in a large extra-tropical climate response (Palmer and Mansfield, 1984).

Ocean–atmosphere interactions in the warm pool are instrumental in triggering El Niño events. Under normal conditions, easterly trade winds, driven by the SST gradient between the east (cool) and west (warm) equatorial Pacific, pile up warm water in the WPWP region. The trades bring moist air, which converges at the WPWP, giving high rainfall in this region. The high rainfall contributes to the relatively low sea surface salinity (SSS), reinforcing the warming of the ocean by restricting ocean mixing. The atmospheric convection above the WPWP releases heat, and facilitates the poleward transfer of heat from the tropics. La Niña is a slight enhancement of normal conditions. During El Niño events, anomalous westerly winds at the edge of the warm pool cause the trade winds to slacken (Fedorov and Philander, 2000). This allows the WPWP to expand eastward, reducing the E–W SST contrast, further slackening the trade winds, and allowing the warm pool to expand even further eastward.

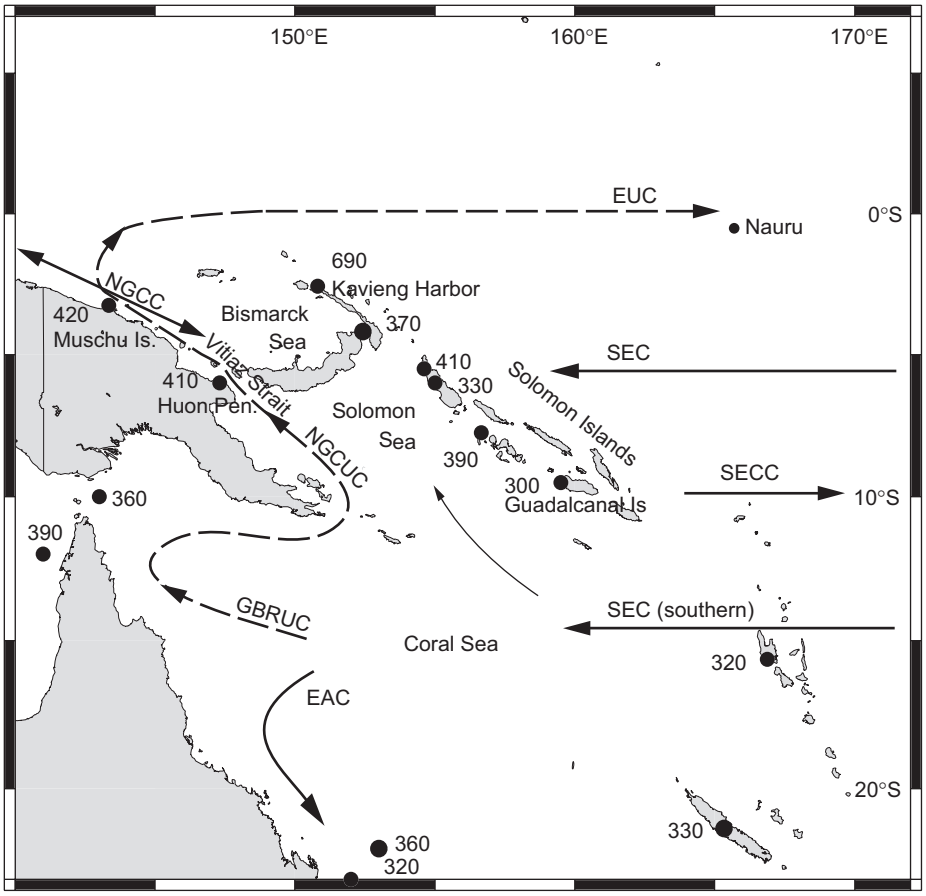

Fig. 2. Diagram showing the major oceanic currents of the western Pacific, present-day reservoir age estimates at sites bordering the Coral, Solomon and Bismark Seas, and selected locations discussed in the text. Figure modified from Fine et al. (1994) and Reverdin et al. (1994). Of significance to the northern coastal PNG region are the equatorial branch of the South Equatorial Current (SEC), the southern branch of the SEC, New Guinea Coastal Undercurrent (NGCUC) and the New Guinea Coastal Current (NGCC). The SEC waters flow into the Coral and Solomon Seas and through the Vitiaz Strait along the north coast of PNG. The NGCUC runs northward along the coast and turns eastward at about 143°E to become the Equatorial Undercurrent (EUC). The EUC strengthens during El Niño events. The NGCC reverses seasonally, depending on the prevailing winds. Reservoir ages are rounded to the nearest decade. Reservoir age data, location information and citations are given in Table 9.

The warm waters of the western tropical Pacific move eastward, producing warm SST anomalies in the east. Atmospheric convection associated with the warm waters is also shifted eastward producing positive rainfall anomalies in the in the central and eastern equatorial Pacific and negative rainfall anomalies in the western tropical Pacific. For the waters around Koil and Muschu Islands, an El Niño event leads to SSS increases, and SST decreases (McGregor and Gagan, 2004) due to displacement of the warm pool and associated convection, and the shoaling of the thermocline inducing mixing with cooler, more saline water (Tourre and White, 1997).

The western tropical Pacific hosts a complex system of ocean currents and undercurrents (Fig. 2; Fine et al., 1994). Of significance in the northern coastal New Guinea region are the SEC, New Guinea Coastal Current (NGCC) and the New Guinea Coastal Undercurrent (NGCUC). West of the date line, southeast trade winds drive the off-equator branch of the westward flowing SEC (centred at ~5°S), which extends to the waters around the Solomon Islands (Reverdin et al., 1994). From there it turns northward feeding the central warm pool waters, and southward forming the weak-flowing South Equatorial Countercurrent (SECC) centred at ~10°S. A second branch of the SEC centred at ~15°S enters the Solomon and Corals Seas introducing sub-tropical gyre water to the area. This most southerly SEC branch bifurcates near 18°S forming the southward East Australia Current (EAC) and the northward flowing Great Barrier Reef Undercurrent (GBRUC; (Tsuchiya et al., 1989). The high-salinity NGCUC has its origins in the GBRUC, and flows northward at a depth of approximately 200 m through the Vitiaz Strait and along the north coast of PNG, finally turning eastward and becoming the Equatorial Undercurrent at about 143°E (Lindstrom et al., 1987), not too far north from Muschu Island. The NGCC is a near-surface current, which flows eastward along the northern PNG coastline during the NW monsoon (January–April) and westward during the SE monsoon (May–August; Fine et al., 1994; Cresswell, 2000), and is directly forced by local winds (Kuroda, 2000).

Outflow from the Sepik River and coastal upwelling are two additional processes that are likely to influence the

northern coastal waters of PNG, in particular the Muschu/Koil region. The Sepik and nearby Ramu Rivers drain the western and central highlands of PNG and combined have the largest catchment area in New Guinea. From 150 m beyond the Sepik River mouth a submarine canyon extends out ~10 km to the 800-m isobath (Cresswell, 2000). Observations from satellite imagery from 1991 to 1997, along with research vessel, moored instruments and drifter data (deployed from 1996 to 1998), and coral proxy data for 1977–1996 showed that during the SE monsoon, the 1–2 m thick Sepik River surface plume is turned westward by the wind-driven NGCC and the opposite occurs in the NW monsoon (Cresswell, 2000; Ayliffe et al., 2004). Upwelling occurs along the north coast of PNG during the NW monsoon and at 143°E high-salinity water was upwelled to the surface from the NGCUC (Cresswell, 2000; Kuroda, 2000). Upwelling was absent during the SE monsoon. Waters at depth, offshore from the Sepik River mouth are stratified into many layers (Cresswell, 2000).

3. Methods

Fossil *Porites* sp. corals were collected in May–June 1998 from Koil and Muschu Islands (Fig. 1). Modern coral MS01, a *Porites lutea* (J.E.N. Veron, personal communication), was collected from a well-flushed fringing reef at Cape Saum, Muschu Island, with its top surface at approximately 5–6 m below mean sea level. The uplifted fossil corals were located in the inter-tidal zone and were eroding out of beach sands (Top Point Beach, Koil Island, and Morock Bay, Muschu Island) or coral rubble/soil (Rebiew Bay, Muschu Island). Locations of individual modern and fossil corals used in this study are given in Table 1. Fossil corals were drilled using tungsten-carbide cutting teeth on the end of a 5-cm diameter core barrel, driven by a chainsaw motor. The modern coral was collected using a hand-held pneumatic drill connected to a 50-mm core barrel with tungsten-carbide cutting teeth and powered by a standard scuba tank. As far as practicable, coral cores were drilled along the major growth axis, and only those drilled on axis were analysed.

Eight fossil corals were selected for radiocarbon and U–Th dating and were chosen on the basis of length, quality of core and geographic spread. Following core selection, all corals were screened for diagenesis using XRD and petrography (see McGregor and Gagan (2003) for detailed methods) to ensure no diagenesis was present. Multiple thin sections were prepared for each coral, except coral FM07 where, since it was only 9-cm long, only one thin section was made. XRD results (Table 1) show that for all corals, the calcite content was below detection limits. The absence of calcite was confirmed by thin section results that show an absence of both calcite and secondary aragonite overgrowths or alteration. A 1912 A.D. sample of modern coral MS01 (age determined independently by growth band counting on a coral X-ray) was included to estimate the modern ocean ^{14}C reservoir correction, calculated using the method of Reimer and Reimer (2001).

For conventional radiocarbon dating, approximately 40 g of material was ultrasonically cleaned then left in 30% (w/v) H_2O_2 for 24 h. Under the direction of staff at the ANU Radiocarbon Dating Laboratory, samples were prepared and counted using the benzene liquid-scintillation method, described in Gupta and Polach (1985). Conventional ^{14}C ages before 1950 A.D. (yr BP) were based on the ANU Sucrose secondary reference standard (Gupta and Polach, 1985). Coral FK05 from Koil Island was dated twice by conventional radiocarbon analysis and showed ages within the 1σ range of each date.

Th/U atomic ratios were determined by isotope dilution methods using a Finnigan MAT-261 thermal ionisation mass spectrometer (TIMS). Initially, 3 g of coralline material was ultrasonically cleaned and dissolved in concentrated nitric acid. Spike "U-2", a mixed ^{229}Th–^{233}U tracer, was added and organic matter removed by the addition of H_2O_2. Uranium and thorium were co-precipitated with iron hydroxide, and then separated in ion exchange columns using HCl. The uranium samples were loaded onto double rhenium filaments and ^{233}U, ^{234}U, ^{235}U and ^{238}U were measured simultaneously in a combined multi-collector/secondary electron multiplier (SEM) system (^{234}U measured in the SEM). To calculate the SEM/Faraday cup relative gain, the $^{238}U/^{235}U$ (^{235}U measured in

Table 1
Location details and XRD results for corals analysed for U–Th and ^{14}C to calculate reservoir ages

Coral	Location	Latitude and longitude	Calcite (%)	Aragonite (%)	Calculation error	Comments
FK05	Koil Island–Top Point Beach	–	0.3	99.7	0.5	BDL
FM24	Muschu Island–Morock Bay	03°24′23″S, 143°36′30″E	0	100	0.5	BDL
FM23	Muschu Island–Morock Bay	03°24′23″S, 143°36′30″E	0.1	99.9	0.3	BDL
FM15	Muschu Island–Morock Bay	03°24′23″S, 143°36′30″E	0	100	0.3	BDL
FM07	Muschu Island–Morock Bay	03°24′23″S, 143°36′30″E	0.1	99.9	0.5	BDL
FM21	Muschu Island–Morock Bay	03°24′23″S, 143°36′30″E	0	100	0.3	BDL
FM22	Muschu Island–Morock Bay	03°24′23″S, 143°36′30″E	0.3	99.7	0.3	BDL
FM09	Muschu Island–Rebiew Bay	03°25′30″S, 143°37′20″E	0.2	99.8	0.0	BDL
MS01	Muschu Island–Cape Saum	03°24′794″S, 143°38′175″E	n/a	n/a		

BDL, below detection limits.

the SEM) was compared to $^{238}U/^{235}U$ (^{235}U measured on the Faraday cup). The ratios $^{234}U/^{235}U$ and $^{233}U/^{235}U$ were corrected for isotopic mass fractionation using the method described in Stirling et al. (1995). The thorium samples were loaded onto single filaments in combination with graphite (used to enhance ionisation) and also run on the Finnigan MAT 261 TIMS. $^{229}Th/^{230}Th$ was measured on the SEM in peak hopping mode. Sample ages were calculated using the Monte Carlo simulation spreadsheet, developed by J. Hellstrom (personal communication) and corrected for non-radiogenic $^{230}Th/^{232}Th$ following the procedures outlined by McCulloch and Mortimer (in press).

Additional samples from seven of the eight corals were taken ~5 cm away from the TIMS U–Th and conventional ^{14}C age dated samples and the age determined by MC-ICPMS U–Th dating. An aliquot was also taken from six of these samples for AMS ^{14}C. Each $3 \times 2 \times 1$ cm block was cleaned several times in deionised water using first an ultrasonic bath and then an ultrasonic probe. The samples were dried for a minimum of 24 h in an oven at ~40 °C before being homogenised using a mortar and pestle.

For MC-ICPMS U–Th dating of the seven additional samples, the carbonate samples were dissolved in HNO_3 and a mixed ^{229}Th–^{233}U spike was added. The Th and U fractions were extracted and separated using a micro ion exchange column (TRU spec resin) and HCl–HF solutions. The U and Th solutions were delivered separately into the ICPMS, and standard plasma operating settings were used. The sample introduction system was thoroughly cleaned using multi-step 2% HNO_3, 0.05% HF and 1% Triton surfactant between each analysis to remove residual ^{230}Th blank. The isotopes ^{229}Th and ^{230}Th were each measured in the central ion counter (with high abundance energy filter (RPQ)) concurrently with ^{232}Th and ^{238}U in Faraday cups, taking advantage of multi-collection measurements in reducing errors from ion beam instabilities. The isotope ^{234}U was also measured in the ion counter concurrently with ^{238}U, ^{235}U, ^{233}U and ^{232}Th in Faraday cups. Mass fractionation corrections for $^{229}Th/^{230}Th$, $^{229}Th/^{232}Th$, $^{234}U/^{238}U$ and $^{233}U/^{238}U$ ratios were undertaken using the naturally occurring ^{235}U and ^{238}U measured simultaneously in Faraday cups. The concentrations of ^{230}Th and ^{238}U were determined using the enriched ^{229}Th and ^{233}U tracers, respectively. Gains were measured statically by measuring $^{234}U/^{235}U$ in the SEM/Faraday system using the SRM 960 standard. The SRM 960 standard was measured at regular intervals (every 1–2 h) depending on instrumental drift and the ultimate stability required for the bracketing of SEM gains. The U baselines were also measured and corrected for tailing. The $^{230}Th/^{238}U$ and $^{234}U/^{238}U$ ratios were measured reproducibly with precisions of ~1–2‰. Results were corrected for the non-radiogenic ^{230}Th component, and for further details of the MC-ICPMS U–Th methods see McCulloch and Mortimer (in press).

A 7–8 mg aliquot of each of the six samples measured by AMS ^{14}C was weighed out and hydrolysed to CO_2 using 85% phosphoric acid, followed by graphitisation using excess H_2 and Fe catalyst as described in Hua et al. (2001). A portion of each graphite sample was used to determine $\delta^{13}C$ for mass fractionation correction. Graphite samples were analysed using the "STAR" 2 MV HVEE tandem accelerator at ANSTO (Fink et al., 2004) with a precision of 0.5–0.6% for mid-Holocene samples and 1.5% for coral FM09.

4. Results

The radiocarbon age of modern coral MS01 was measured to calculate the oceanic ^{14}C reservoir age for the northern coastal PNG. The reservoir age for pre-1950 A.D. aged marine samples is calculated as follows:

$$R = {}^{14}\text{C age (measured)} - \text{atmospheric } {}^{14}\text{C age}, \quad (1)$$

where R is the reservoir age, and the atmospheric ^{14}C age is the calendar age of the sample (calculated independently), converted to a ^{14}C age based on the IntCal04 calibration curve (Reimer et al., 2004).

Local offsets (ΔR) from the global average reservoir age calculated as follows:

$$\Delta R = {}^{14}\text{C age (measured)} - \text{marine model age}, \quad (2)$$

where the marine model age is the calendar age of the sample (calculated independently), converted to a ^{14}C age based on the Marine04 curve (Hughen et al., 2004).

For modern coral MS01, the measured ^{14}C age was 520 ± 60 yr BP, and the band-counted calendar age was

Table 2
MS01 reservoir age and ΔR calculation

	Calendar age	Conventional ^{14}C age[a] (yr BP)	$\Delta^{14}C$ (‰) $\pm 1\sigma$	Atmospheric ^{14}C age[b] (yr BP)	Marine model age[a] (yr BP)	R^c (^{14}C yr)	ΔR^d (^{14}C yr)
MS01	1912 A.D.	520 ± 60	-58 ± 7	100 ± 7	450 ± 23	420 ± 60	70 ± 60

All errors $\pm 1\sigma$.
[a]Conventional ^{14}C date measured in this study.
[b]From IntCal04 (atmospheric) (Reimer et al., 2004) and Marine04 (marine) (Hughen et al., 2004). Data available from website ⟨http://www.radiocarbon.org/IntCal04.htm⟩.
[c]Calculated using Eq. (1).
[d]Calculated using Eq. (2).

1912 A.D. This gave a reservoir correction of 420 ± 60 ^{14}C yr (Table 2). ΔR for MS01 is 70 ± 60 ^{14}C yr (Table 2).

TIMS and MC-ICPMS U–Th ages are presented in Tables 3 and 4, respectively, along with $\delta^{234}U(t)$ results for each dataset. $\delta^{234}U(t)$ values are within the range expected for pristine coral aragonite (Stein et al., 1993; Stirling et al., 1995; Hughen et al., 2004). Of the seven samples that have both TIMS and MC-ICPMS U–Th age estimates, all are within error (2σ), except for FM09. Samples with radiocarbon ages <5400 yr BP have MC-ICPMS U-series age older than the corresponding TIMS U-series age (Table 3 compared with Table 4).

Results from the conventional and AMS radiocarbon dating of the fossil coral are presented in Table 5. All conventional and AMS radiocarbon ages for the six samples dated by both methods are within error (1σ), giving confidence in the radiocarbon results.

All radiocarbon data were converted to Δ^{14}C, with the paired TIMS U–Th and conventional ^{14}C ages treated as

Table 3
TIMS U–Th results for fossil corals

Sample	U (ppm)	^{230}Th/^{238}U $\times 10^4$ (activity)	$\delta^{234}U(t)$	^{230}Th/^{232}Th (activity)	U–Th age (yr)	U–Th age ^{230}Th/^{232}Th corrected (yr)	U–Th age (yr BP)
FK05	3.4	779 ± 5	148 ± 1	8515	7650 ± 45	7650 ± 45	7600 ± 45
FM24	3.22	742 ± 9	148 ± 1	1420	7270 ± 75	7260 ± 80	7210 ± 80
FM23	2.99	725 ± 16	147 ± 1	477	7100 ± 145	7090 ± 160	7040 ± 160
FM15	3.11	625 ± 6	148 ± 1	422	6090 ± 50	6075 ± 65	6025 ± 65
FM07	3.19	603 ± 17	146 ± 1	677	5880 ± 160	5870 ± 170	5820 ± 170
FM21	3.23	603 ± 11	151 ± 1	1919	5850 ± 100	5850 ± 105	5800 ± 105
FM22	3.41	555 ± 14	150 ± 2	933	5380 ± 130	5370 ± 135	5320 ± 135
FM09	3.03	214 ± 6	147 ± 1	41	2040 ± 50	1990 ± 100	1940 ± 100

U–Th age determinations were made in 2000 A.D. and on the same samples as for the conventional radiocarbon ages. U–Th ages were corrected for the non-radiogenic ^{230}Th component, based on non-radiogenic ^{230}Th/^{232}Th $= 1 \pm 1$ (McCulloch and Mortimer, in press). The U–Th ages quoted in yr BP have been calculated relative to 1950 A.D. for comparison with radiocarbon results. All errors are $\pm 2\sigma$.

Table 4
MC-ICPMS U–Th results for fossil corals

Sample	U (ppm)	^{230}Th/^{238}U $\times 10^4$ (activity)	$\delta^{234}U(t)$	^{230}Th/^{232}Th (activity)	U–Th age (yr)	U–Th age ^{230}Th/^{232}Th corrected (yr)	U–Th age (yr BP)
FK05	2.35	771 ± 5	149 ± 2	844	7560 ± 55	7550 ± 60	7495 ± 60
FM24	2.20	745 ± 4	149 ± 1	396	7305 ± 40	7290 ± 55	7230 ± 55
FM23	2.11	727 ± 5	150 ± 1	206	7120 ± 50	7090 ± 80	7030 ± 80
FM15	–	–	–	–	–	–	–
FM07	2.27	612 ± 4	149 ± 1	176	5955 ± 40	5920 ± 75	5865 ± 75
FM21	2.12	608 ± 4	148 ± 2	218	5925 ± 35	5900 ± 65	5840 ± 65
FM22	2.26	569 ± 5	148 ± 1	280	5530 ± 50	5510 ± 70	5455 ± 70
FM09	2.06	235 ± 4	150 ± 1	169	2250 ± 40	2235 ± 50	2180 ± 50

U–Th age determinations were made in 2007 A.D. and on the same samples as for the AMS radiocarbon ages. U–Th ages were corrected for the non-radiogenic ^{230}Th component, based on non-radiogenic ^{230}Th/^{232}Th $= 1 \pm 1$ (McCulloch and Mortimer, in press). The U–Th ages quoted in yr BP have been calculated relative to 1950 A.D. for comparison with radiocarbon results, and rounded to the nearest half decade. All errors are $\pm 2\sigma$.

Table 5
Conventional and AMS radiocarbon ages for fossil corals

Sample No.	Conventional ^{14}C data		AMS ^{14}C data	
	ANU Lab Code	Conventional ^{14}C age (yr BP) $\pm 1\sigma$	ANSTO Lab Code	AMS ^{14}C Age (yr BP) $\pm 1\sigma$
FK05-a	ANU-11061	7470 ± 80	OZJ424	7480 ± 35
FK05-b	ANU-11061B	7330 ± 80	n/a	n/a
FM24	ANU-11203	6520 ± 70	OZJ430	6425 ± 35
FM23	ANU-11196	6270 ± 60	OZJ429	6280 ± 35
FM15	ANU-11060	5400 ± 80	–	–
FM07	ANU-11201	5350 ± 80	–	–
FM21	ANU-11198	5740 ± 70	OZJ427	5675 ± 35
FM22	ANU-11059	5090 ± 70	OZJ428	5125 ± 30
FM09	ANU-11056	2280 ± 60	OZJ426	2370 ± 35

one dataset, (termed TIMS-CONV; Table 6), and the paired MC-ICPMS U–Th and AMS ^{14}C ages treated as another dataset, (termed MC-ICPMS-AMS; Table 7). Fossil coral Δ^{14}C for TIMS-CONV and MC-ICPMS-AMS, where Δ^{14}C is the decay corrected ^{14}C/^{12}C relative to the internationally agreed 1950 standard value, are offset compared to Δ^{14}C for Marine04 and IntCal04 (Fig. 3). The difference in Δ^{14}C for the corals and Marine04 represents ΔR (when expressed radiocarbon years (^{14}C yr)), and the difference between Δ^{14}C for the corals and IntCal04 represents the reservoir age (again when expressed in ^{14}C yr). The Δ^{14}C results suggest that in general, reservoir ages and ΔR for the mid-Holocene at this site are lower than at present.

Table 6
Calculation of TIMS-conventional ^{14}C reservoir age (R) and ΔR

Sample	U–Th age (yr BP)	Conventional ^{14}C age[a] (^{14}C yr BP)	Δ^{14}C[b] (‰)	Atmospheric ^{14}C age[c] (^{14}C yr BP)	Marine model age[d] (^{14}C yr BP)	R[e] (^{14}C yr)	ΔR[f] (^{14}C yr)
FK05	7600±23	7400±70[g]	−2±12	6755±45	7135±7	645±85	265±70
FM24	7210±40	6520±70	62±15	6275±23	6683±38	245±75	−165±80
FM23	7040±80	6270±60	73±19	6175±40	6518±57	95±70	−250±85
FM15	6025±33	5400±70	58±15	5305±35	5634±1	95±85	−235±80
FM07	5820±85	5350±80	38±21	5065±55	5453±74	285±95	−105±110
FM21	5800±53	5740±80	−14±15	5070±28	5425±34	670±75	315±80
FM22	5320±68	5090±70	10±17	4630±118	4955±43	460±135	135±80
FM09	1940±50	2280±60	−48±13	1990±38	2331±34	290±70	−50±70

For comparison, the modern R is 420±60 ^{14}C yr. U–Th age and conventional ^{14}C age errors are ±1σ.

[a]Conventional ^{14}C dates measured in this study.

[b]Δ^{14}C is the decay corrected ^{14}C/^{12}C relative to the internationally agreed 1950 standard value. The Δ^{14}C error is the span of the maximum and minimum Δ^{14}C equivalent to the U–Th (1σ) age range.

[c]U–Th age was converted to atmospheric ^{14}C age graphically similar to Southon et al. (1995), using the IntCal04 (atmospheric) curve (Reimer et al., 2004; http://www.radiocarbon.org/IntCal04.htm). The atmospheric ^{14}C age is the median of the oldest and youngest ^{14}C ages equivalent to the U–Th (1σ) age range. The atmospheric ^{14}C age error is the span of the oldest and youngest ^{14}C ages. Ages were rounded to the nearest half decade.

[d]The marine model age and error quoted here is such that, using CALIB v5.0.1 (Stuiver et al., 2005), Marine04 data (Hughen et al., 2004) and $\Delta R = 0$ will give a calibrated age (1σ) equivalent to the U–Th age (1σ) range.

[e]R was calculated using Eq (1). The 1σ error is $\left(1\sigma^2_{\text{atmospheric }^{14}\text{C age}} + 1\sigma^2_{\text{Conventional }^{14}\text{C age}}\right)^{1/2}$.

[f]ΔR was calculated using Eq. (2). The 1σ error is $\left(1\sigma^2_{\text{marine model age}} + 1\sigma^2_{\text{Conventional }^{14}\text{C age}}\right)^{1/2}$.

[g]Mean and standard error of the two analyses of this coral.

Table 7
Calculation of MC-ICPMS-AMS ^{14}C reservoir age (R) and ΔR

Sample	U–Th age (yr BP)	AMS ^{14}C age[a] (^{14}C yr BP)	Δ^{14}C[b] (‰)	Atmospheric ^{14}C age[c] (^{14}C yr BP)	Marine model age[d] (^{14}C yr BP)	R[e] (^{14}C yr)	ΔR[f] (^{14}C yr)
FK05	7495±30	7480±35	−24±8	6610±43	7000±15	870±55	480±40
FM24	7230±30	6425±35	78±8	6275±28	6699±12	150±45	−275±35
FM23	7030±40	6280±35	71±10	6175±35	6518±1	105±50	−240±35
FM15	–	–					
FM07	–	–					
FM21	5840±30	5675±35	0±8	5053±20	5456±15	620±40	220±40
FM22	5455±70	5125±30	22±8	4690±83	5087±21	435±90	40±35
FM09	2180±50	2370±35	−31±7	2215±23	2509±6	155±40	−140±35

For comparison, the modern R is 420±60 ^{14}C yr. MC-ICPMS U–Th age and AMS ^{14}C age errors are ±1σ.

[a]Conventional ^{14}C dates measured in this study.

[b]Δ^{14}C is the decay corrected ^{14}C/^{12}C relative to the internationally agreed 1950 standard value. The Δ^{14}C error is the span of the maximum and minimum Δ^{14}C equivalent to the U–Th (1σ) age range.

[c]U–Th age was converted to atmospheric ^{14}C age graphically similar to (Southon et al., 1995), using the IntCal04 (atmospheric) curve (Reimer et al., 2004; http://www.radiocarbon.org/IntCal04.htm). The atmospheric ^{14}C age is the median of the oldest and youngest ^{14}C ages equivalent to the U–Th (1σ) age range. The atmospheric ^{14}C age error is the span of the oldest and youngest ^{14}C ages. Ages were rounded to the nearest half decade.

[d]The marine model age and error quoted here is such that, using CALIB v5.0.1 (Stuiver et al., 2005), Marine04 data (Hughen et al., 2004), and $\Delta R = 0$ will give a calibrated age (1σ) equivalent to the U–Th age (1σ) range.

[e]R was calculated using Eq. (1). The 1σ error is $\left(1\sigma^2_{\text{atmospheric }^{14}\text{C age}} + 1\sigma^2_{\text{Conventional }^{14}\text{C age}}\right)^{1/2}$.

[f]ΔR was calculated using Eq. (2). The 1σ error is $\left(1\sigma^2_{\text{atmospheric }^{14}\text{C age}} + 1\sigma^2_{\text{Conventional }^{14}\text{C age}}\right)^{1/2}$.

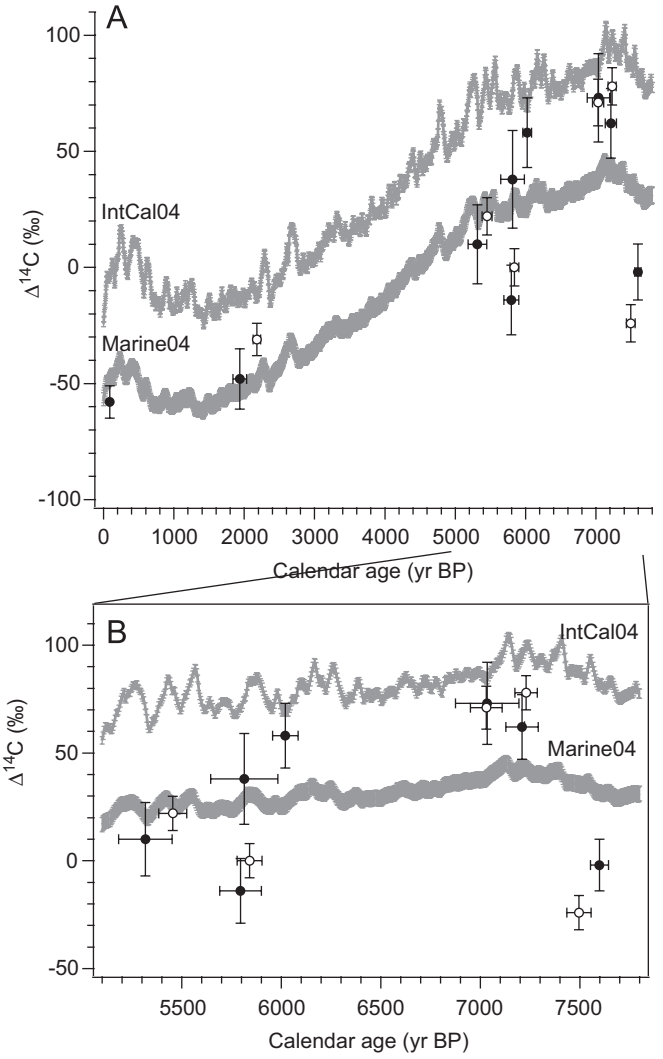

Fig. 3. Comparison of $\Delta^{14}C$ for fossil corals and the IntCal04 (Reimer et al., 2004) and Marine04 (Hughen et al., 2004) calibration curves. (A) Complete fossil and modern coral $\Delta^{14}C$ dataset. Coral $\Delta^{14}C$ from conventional radiocarbon dating (filled circles) are from Tables 2 and 6. Coral $\Delta^{14}C$ are plotted against the corresponding TIMS U–Th age in yr BP relative to 1950 A.D. for the fossil corals, and against the band-counted calendar age for the modern coral. Coral $\Delta^{14}C$ from AMS radiocarbon analysis (open circles) are from Table 7, and are plotted against the corresponding MC-ICPMS U–Th age in yr BP relative to 1950 A.D. The $\Delta^{14}C$ error is the span of the maximum and minimum $\Delta^{14}C$ equivalent to the U–Th (1σ) age range. U–Th dates are plotted with 2σ errors. If the error bars are not visible then they are smaller than the size of the symbol. The IntCal04 and Marine04 data are plotted with their 1σ errors. (B) As for part (A) except zooming in on the early to mid-Holocene period.

To explore the mid-Holocene changes further, differences between the fossil coral ^{14}C and U–Th dates were used to calculate reservoir ages and ΔR. These were calculated using Eqs. (1) and (2), and atmospheric and marine ^{14}C ages based on U–Th dates. Again TIMS-CONV data were treated as one dataset (Table 6) and MC-ICPMS-AMS as another (Table 7) for the calculations. Finally, a weighted mean U-series age, ΔR and reservoir age estimate were calculated for each coral using a random effects model (Table 8; Fig. 4A and B). Although both reservoir age and ΔR were calculated, results will be discussed in terms of reservoir age to facilitate comparison with results from other locations.

The summary results show that at a weighted average U–Th age of 7550 ± 35 yr BP, the reservoir age for this Koil Island coral is $365\ ^{14}C$ yr older than present (785 ± 75 compared with $420\ ^{14}C$ yr; Table 8). It is difficult to know how reliable this result is given that reservoir age estimates from TIMS-CONV and MC-ICPMS-AMS do not overlap (hence the large error on the weighted mean for this coral, and the over-dispersion (Table 8)), though they both show the same trend toward large reservoir ages. This coral comes from a different island to the other coral samples, and this coral is older, so additional samples from this site should be measured to confirm this result.

From 7220 to 5850 yr BP, the weighted average reservoir age is $185 \pm 30\ ^{14}C$ yr ($n = 4$; calculated using the random effects model), and returns to modern values at 5420 ± 35 yr BP (Fig. 4B). The reservoir age for coral FM21 of 635 ± 35 at 5830 ± 35 yr BP, though, appears too large compared to the similar aged coral FM07 ($R = 285 \pm 95$ at 5855 yr BP; Table 8) and one or both of these corals could be giving erroneous results. However, unlike corals FK05 and FM09 (discussed below), comparison of FM21 and FM07 TIMS and MC-ICPMS U–Th ages are within error (Tables 6 and 7). Conventional ^{14}C and AMS ^{14}C results for FM21 also show ages within error (Table 5). FM07 was not dated by AMS ^{14}C. Overall, this suggests that the U–Th and ^{14}C data are sound, and it may indicate that reservoir ages are more variable than previously thought. If on the other hand FM07 and FM21 are giving spurious data, then this does not alter the result of low reservoir ages between 7220 and 5850 yr BP found in this study, as this result is supported by three additional coral reservoir age estimates.

The reservoir age at 2065 ± 85 yr BP, of $215 \pm 50\ ^{14}C$ yr, is based on analysis of a single fossil coral (FM09). Neither the 2σ U–Th ages nor the reservoir age errors for the TIMS-CONV and MC-ICPMS-AMS datasets overlap for this coral (Tables 6 and 7). Results from this coral should be treated with caution. Coral FM09 should be further investigated for diagenesis, a possible source of error, and analyses of similar-aged corals from this location should be undertaken to clarify this result.

5. Discussion

ΔR for modern coral MS01 ($70 \pm 60\ ^{14}C$ yr) is half that estimated by Stuiver and Braziunas (1993) for the tropical western Pacific. However reservoir age for MS01 of $420\ ^{14}C$ yr, is similar to that of 400 and $410\ ^{14}C$ yr, calculated by Chappell and Polach (1991) and Edwards et al. (1993), respectively, for nearby Huon Peninsula, PNG (Fig. 2, Table 9). The Muschu Island reservoir age is older (though within error) than the majority of modern reservoir ages calculated for samples from islands

Table 8
Summary of PNG U–Th ages and reservoir age estimates for each coral

Sample no.	U–Th age (yr BP)	U–Th S.E. (yr BP)	Reservoir age (^{14}C yr)	Reservoir age S.E. (^{14}C yr)	ΔR (^{14}C yr)	ΔR S.E. (^{14}C yr)
FK05	7550	35	785	75	455	35
FM24	7215	35	190	40	−265	35
FM23	7030	35	100	40	−240	30
FM15	6025	30	95	85	−235	80
FM07	5855	35	285	95	−105	110
FM21	5830	25	635	35	245	35
FM22	5420	35	445	75	95	50
FM09	2065	85	215	50	−135	35

Where both TIMS-CONV and MC-ICPMS-AMS datasets exist for each coral a weighted mean average and standard error (S.E.) were estimated for each parameter, including U–Th (S.E. based on the 1σ errors), using a random effects model (Galbraith and Laslett, 1993; Galbraith et al., 1999). Coral FM09 showed over-dispersion of 18% using the random effects model and the U–Th age and R estimates should be treated with caution. Likewise, the reservoir age estimate for FK05 showed 10% over-dispersion. Values for FM15 and FM07 are the TIMS-CONV values and 1σ error. All data were rounded to the nearest half decade.

bordering the Bismark, Solomon and Coral Seas (Fig. 2, Table 9; Gillespie and Polach, 1979; Druffel and Griffin, 1993, 1999; Guilderson et al., 2004; Petchey et al., 2004) and is older than the reservoir age modelled for the present-day north coast of PNG (Butzin et al., 2005). Most Coral Sea and southern Solomon Sea sites receive their ^{14}C signal from the well-equilibrated southern-most branch of the SEC (centred at ~15°S) with origins in the sub-tropical gyre (Druffel and Griffin, 1993, 1999; Reverdin et al., 1994; Guilderson et al., 2004). Those sites in the Bismark Sea and northern Solomon Sea receive their signal from the south equatorial branch of the SEC (Reverdin et al., 1994; Petchey et al., 2004). Sub-annual ^{14}C analysis of modern corals from Nauru and Guadalcanal Island (see Fig. 2 for locations) suggests that the equatorial SEC originates in the depleted ^{14}C waters of the eastern equatorial Pacific (Guilderson et al., 1998, 2000, 2004). Kavieng Harbor, New Ireland, is the exception to this general pattern and gave a reservoir age of 690 ^{14}C yr due to local upwelling (Petchey et al., 2004). It is likely that Muschu Island receives its ^{14}C signal via equatorial SEC waters from the Solomon Sea, delivered primarily through the Viatiaz Strait. The Muschu Island waters may also be influenced by NGCUC waters upwelled during the NW monsoon.

The most striking feature of the Muschu and Koil Island mid-Holocene results is the low reservoir ages, averaging 185 ± 30 ^{14}C yr ($n = 4$), found for samples U–Th dated between 7220 and 5850 yr BP (Fig. 4A). These reservoir ages are 235 ^{14}C yr younger than the modern reservoir age of 420 ^{14}C yr. Such low reservoir ages are not unprecedented at least in the modern ocean. Sites bordering on the South China Sea (SCS), also within the WPWP, are influenced by the high ^{14}C waters of the Pacific North Equatorial Current (PNEC) and, depending on the season, SEC waters also relatively high in ^{14}C (Southon et al., 2002). The high ^{14}C waters entering the SCS, restricted upwelling, and with efficient air–sea gas exchange, combine to give low reservoir ages, as low as 141 ± 50 ^{14}C yr (Southon et al., 2002). If similar well-equilibrated surface ocean waters were reaching the north coast of PNG, and coastal upwelling was suppressed, then this could give rise to low reservoir ages.

Changes in the oceanic reservoir ages found for the PNG Holocene corals could indicate changes in oceanic processes or a change in the ^{14}C of the source waters for the ocean currents. At this stage, little is known of the source water ^{14}C variability during the Holocene so we assume that our changes are due to changes in ocean circulation.

The low reservoir ages from 7220 to 5850 yr BP suggest that water well-equilibrated with the atmospheric ^{14}C reached the northern coastal PNG region. One possibility could be a suppression of upwelling during the NW monsoon along the north coast of PNG. The reservoir age data presented here are not sufficiently resolved to detect such seasonal changes so this possibility cannot be ruled out.

Another possibility is an increase in well-equilibrated Sepik River waters reaching Muschu Island. Dating and mapping of Sepik floodplain sediments suggests that at 6000 cal yr BP an inland sea existed in the Sepik–Ramu lowlands, and this sea infilled steadily to present (Swadling et al., 1989; Chappell, 1993). It is unlikely however that the Sepik flood plume exerted a greater influence on the Muschu corals than today; δ^{18}O-based SSS estimates suggest more saline conditions at Muschu Island at this time (McGregor, 2003) and a reduced river discharge. In addition, even if the river discharge was greater than today, the signal may not have reached Muschu Island because mixing of ocean and river water occurred in the inland sea (Swadling et al., 1989; Chappell, 1993).

The lower reservoir ages during the early to mid-Holocene could reflect changes in ocean circulation in the western equatorial Pacific due to the La Niña-like conditions dominant at the time. Both modelling and palaeoclimate studies suggest a reduction of El Niño frequency and

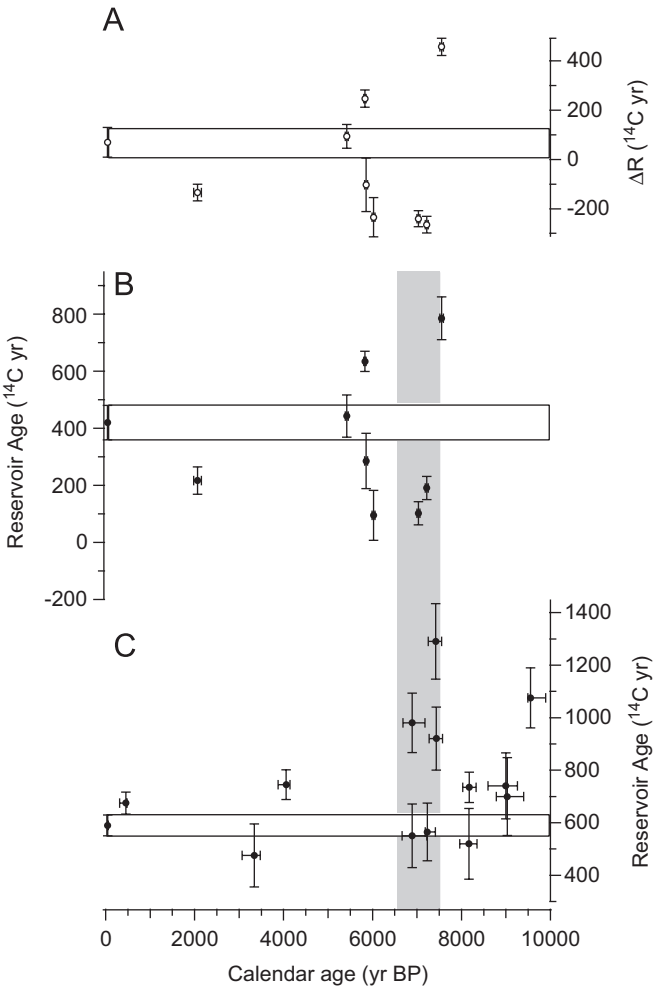

Fig. 4. Weighted average Holocene oceanic ΔR and ^{14}C reservoir ages for Muschu and Koil Island corals and reservoir ages for the Peruvian margin. (A) Muschu and Koil coral weighted mean ΔR and standard errors from Table 8. Calendar ages are weighted mean U–Th dates and standard errors, also from Table 8. (B) Muschu and Koil coral weighted mean reservoir ages. Reservoir ages and standard errors, plus U–Th weighted mean calendar ages are from Table 8. The horizontal box shows modern reservoir age with 1σ error. The ^{14}C reservoir ages have varied significantly through the Holocene. (C) Reservoir age estimates based on radiocarbon dating of contemporaneous terrestrial organic-rich layers and marine shells from Quebreda de los Burros, southern Peruvian coast (Fontugne et al., 2004). Calendar ages are the calibrated age ranges of the terrestrial material. The horizontal box shows modern reservoir age and its associated error. The grey box indicates where the Muschu and Koil Island data and Peruvian datasets cover the same period.

amplitude during the early to mid-Holocene (Bush, 1999; Rodbell et al., 1999; Clement et al., 2000; Liu et al., 2000; Tudhope et al., 2001; Moy et al., 2002; Gagan et al., 2004; McGregor and Gagan, 2004), and that an average La Niña-like state prevailed (Koutavas et al., 2002). Reservoir ages in the eastern Pacific, calculated from contemporaneous Peruvian coast terrestrial and marine samples, appear to respond to the ENSO state in the tropical Pacific and show increases during the early to mid-Holocene (Fig. 4B). This signifies an increase in upwelling intensity at this time and is consistent with a La Niña state. During La Niña events today, Peruvian upwelling intensifies due in part to stronger easterly trade winds, and this brings more ^{14}C depleted water ("older" water) to the surface ocean.

Generally lower reservoir ages in the PNG corals broadly correspond to higher reservoir ages on the Peruvian coast (Fig. 4), and the low reservoir ages in the PNG corals could indicate increased flow of well-equilibrated sub-tropical waters from the southern branch of the SEC. During La Niña-like conditions of the early to mid-Holocene, trade winds are thought to have strengthened and the intertropical convergence zone (ITCZ) likely sat further north than its present position due to greater summer insolation in the northern hemisphere (Liu et al., 2000; Stott et al., 2004). Strengthened trade winds would enhance air–sea exchange rates in the southern SEC reducing the ^{14}C age of this water. The southern branch of the SEC may also have sat further north than at present due to the northward shift in the ITCZ also contributing well-equilibrated surface waters to the northern coastal PNG region. These factors, combined with a possible reduction in PNG coastal upwelling during the NW monsoon, may have caused the reduced reservoir ages observed between 7220 and 5850 yr BP.

From 5850 yr BP to approximately 5420 yr BP, reservoir ages return to modern values (Fig. 4B). This is in agreement with a modern reservoir age for a 6000-yr-old coral from Vanuatu (Paterne et al., 2004). The timing of this transition is similar to the increase in frequency of strong El Niño events beginning in the mid-Holocene inferred from analysis of the recurrence of El Niño-related lake deposits in South America (Rodbell et al., 1999; Moy et al., 2002). The timing is also similar to a shift to higher charcoal (increased fire occurrence) found in terrestrial cumulative charcoal records from the Indonesia/PNG area (Haberle et al., 2001). The changes in the charcoal record are attributed to increased ENSO variability after 5000 yr BP (Haberle et al., 2001; Gagan et al., 2004). Planktonic foraminifera stable isotope records from the western Pacific Ocean show higher variability also attributed to increased El Niño activity (Brijker et al., 2007).

Sub-annual ^{14}C analyses of modern corals from the Solomon and Coral Seas show that during El Niño events today, the equatorial branch of the SEC is displaced southwards bringing ^{14}C depleted equatorial waters to these seas (Druffel and Griffin, 1993, 1999; Guilderson et al., 2004). Trade winds also slacken during El Niño events reducing air–sea exchange. With an increase in El Niño frequency from approximately 6000–5000 yr BP, the equatorial SEC could be displaced southward more often bringing ^{14}C-depeleted waters from the equator and into the Coral and Solomon Seas. These waters would flow through the Vitiaz Strait transferring the signal to coastal New Guinea waters and increasing reservoir ages in the Muschu Island corals. Strengthened coastal PNG upwelling of NGCUC waters at this time could also contribute to the higher reservoir ages.

Table 9
Reservoir age and location information for sites bordering the Coral, Solomon and Bismarck Seas

Location	Latitude	Longitude	Reference	Reservoir age (^{14}C yr)
Muschu Island, PNG	03°25′S	143°35′E	This study	420±60
Huon Peninsula, PNG	06°S	147°30′E	Edwards et al. (1993)	407±52
Kavieng Harbor, New Ireland ($n = 8$)	02°57′S	150°80′E	Petchey et al. (2004)	690±60
Duke of York Island; St. Georges Channel	04°17′S	152°42′E	Petchey et al., 2004)	372±68
Teop Island	05°50′S	154°62′E	Petchey et al., 2004)	406±46
Bougainville	06°00′S	155°00′E	Petchey et al., 2004)	329±41
Vella Lavella Island	07°75′S	156°65′E	Petchey et al., 2004)	389±41
Guadalcanal Island	09°50′S	159°50′E	Guilderson et al. (2004)	302±30
Torres Strait ($n = 3$)	10°00′S	143°00′E	Gillespie and Polach (1979)	361±80
Gulf of Carpentaria ($n = 2$)	12°00′S	141°00′E	Rhodes et al. (1980)	386±60
Espirtu Santo, Vanuatu	15°63′S	166°88′E	Burr et al. (1998)	317±18
New Caledonia ($n = 2$)	21°33′S	165°33′E	Petchey et al. (2004)	326±46
Abraham Reef (Great Barrier Reef)	22°10′S	153°00′E	Druffel and Griffin (1993, 1999)	357±9
Heron Island (Great Barrier Reef)	23°00′S	152°00′E	Druffel and Griffin (1993, 1999)	322±10

All data except that from Edwards et al. (1993) were accessed from the CHRONO Marine Reservoir Database (http://calib.qub.ac.uk/marine/index.php; Reimer and Reimer (2001)).

6. Conclusion

The oceanic ^{14}C reservoir ages for Koil and Muschu Island, PNG show marked changes during the middle Holocene. Relatively low reservoir ages occur between 7220 and 5850 yr BP, which may reflect the influence of well-equilibrated sub-tropical waters at the site. These sub-tropical waters may have been laterally advected to the site via the southern branch of the SEC. This is consistent with strengthened trade winds (facilitating air–sea exchange) and a more northerly position of the Intertropical Convergence Zone under the influence of a more La Niña-like climate state in the Pacific at this time. Reservoir ages similar to modern values between 5850 and 5420 yr BP could represent the onset of modern ocean circulation patterns as El Niño events became more common.

Acknowledgements

We thank the crew of the RV Lady Basten and Irena Zagorskis, James True, Jonathon Allen, George Maiet and Tim Rowland for their help with coral surveying and drilling on the islands off the Wewak coast. Abaz Almanovic and Damien Kelleher are thanked for running the conventional radiocarbon samples, and thanks also to Vladimir Levchenko for assistance with AMS analyses. Emma-Kate Potter is gratefully acknowledged for assistance with measuring U–Th samples on the TIMS. This manuscript benefited from discussions with Quan Hua and Bert Roberts and thoughtful comments from two anonymous reviewers. This work was supported by an Australian Postgraduate Award to H.V.M. Fieldwork was funded by Project TROPICS (Tropical River–Ocean Processes in Coastal Settings), and AMS dates were funded by the ANSTO 'Cosmogenic climate Archives of the Southern Hemisphere' (CcASH) Project.

Editorial handling by: Y. Yokoyama

References

Adkins, J.F., Cheng, H., Boyle, E.A., Druffel, E.R.M., Edwards, R.L., 1998. Deep-sea coral evidence for rapid change in ventilation of the deep North Atlantic 15,400 years ago. Science 280, 725–728.

Ayliffe, L.K., Bird, M.I., Gagan, M.K., Isdale, P.J., Scott-Gagan, H., Parker, B., Griffin, D., Nongkas, M., McCulloch, M.T., 2004. Geochemistry of coral from Papua New Guinea as a proxy for ENSO ocean–atmosphere interactions in the Pacific Warm Pool. Continental Shelf Research 24, 2343–2356.

Brijker, J.M., Jung, S.J.A., Ganssen, G.M., Bickert, T., Kroon, D., 2007. ENSO related decadal scale climate variability from the Indo-Pacific Warm Pool. Earth and Planetary Science Letters 253, 67–82.

Burr, G.S., Beck, J.W., Taylor, F.W., Récy, J., Edwards, R.L., Cabioch, G., Corrége, T., Donahue, D.J., O'Malley, J.M., 1998. A high-resolution radiocarbon calibration between 11,700 and 12,400 calendar years BP derived from ^{230}Th ages of corals from Espiritu Santo Island, Vanuatu. Radiocarbon 40, 1093–1105.

Bush, A.B.G., 1999. Assessing the impact of Mid-Holocene insolation on the atmosphere–ocean system. Geophysical Research Letters 26, 99–102.

Butzin, M., Prange, M., Lohmann, G., 2005. Radiocarbon simulations for the glacial ocean: the effects of wind stress, Southern Ocean sea ice and Heinrich events. Earth and Planetary Science Letters 235, 45–61.

Chappell, J., 1993. Contrasting Holocene sedimentary geologies of lower Daly River, northern Australia, and lower Sepik–Ramu, Papua New Guinea. Sedimentary Geology 83, 339–358.

Chappell, J., Polach, H., 1991. Post-glacial sea-level rise from a coral record at Huon Peninsula, Papua New Guinea. Nature 349, 147–149.

Clement, A.C., Seager, R., Cane, M.A., 2000. Suppression of El Niño during the mid-Holocene by changes in the Earth's orbit. Paleoceanography 15, 731–737.

Cresswell, G.R., 2000. Coastal currents of northern Papua New Guinea, and the Sepik River outflow. Marine Freshwater Research 51, 553–564.

Druffel, E.R.M., Griffin, S., 1993. Large variations of surface ocean radiocarbon: evidence of circulation changes in the southwestern Pacific. Journal of Geophysical Research 98, 20249–20259.

Druffel, E.R.M., Griffin, S., 1999. Variability of surface ocean radiocarbon and stable isotopes in the southwestern Pacific. Journal of Geophysical Research 104, 23607–23613 doi: 0148-0227/99/1999 JC900212.

Edwards, R.L., Beck, J.W., Burr, G.S., Donahue, D.J., Chappell, J.M.A., Bloom, A.L., Druffel, E.R.M., Taylor, F.W., 1993. A large drop in atmospheric $^{14}C/^{12}C$ and reduced melting in the Younger Dryas, documented with ^{230}Th ages of corals. Science 260, 962–968.

Fedorov, A.V., Philander, S.G., 2000. Is El Nino changing? Science 288, 1997–2002.

Fine, R.A., Lukas, R., Bingham, F.M., Warner, M.J., Gammon, R.H., 1994. The western equatorial Pacific: a water mass crossroads. Journal of Geophysical Research 99, 25063–25080.

Fink, D., Hotchkis, M., Hua, Q., Jacobsen, G., Smith, A.M., Zoppi, U., Child, D., Mifsud, C., van der Gaast, H., Williams, A., Williams, M., 2004. The ANTARES AMS facility at ANSTO. Nuclear Instruments and Methods in Physics Research Section B: Beam Interactions with Materials and Atoms 223/224, 109–115.

Fontugne, M., Carré, M., Bentaleb, I., Julien, M., Lavallée, D., 2004. Radiocarbon reservoir age variations in the south Peruvian upwelling during the Holocene. Radiocarbon 46, 531–537.

Gagan, M.K., Hendy, E.J., Haberle, S.G., Hantoro, W.S., 2004. Post-glacial evolution of the Indo-Pacific Warm Pool and El Niño–Southern Oscillation. Quaternary International 118/119, 127–143.

Galbraith, R.F., Laslett, G.M., 1993. Statistical models for mixed fission track ages. Nuclear Tracks and Radiation Measurements 21, 459–470.

Galbraith, R.F., Roberts, R.G., Laslett, G.M., Yoshida, H., Olley, J.M., 1999. Optical dating of single and multiple grains of quartz from Jinmium rock shelter, northern Australia: part 1, experimental design and statistical models. Archaeometry 41, 339–364.

Gillespie, R., Polach, H.A., 1979. In: Berger, R., Suess, H.E. (Eds.), Radiocarbon Dating; Proceedings of the Ninth International Conference. UCLA, pp. 404–421.

Guilderson, T.P., Schrag, D.P., Kashgarian, M., Southon, J., 1998. Radiocarbon variability in the western equatorial Pacific inferred from a high-resolution coral record from Nauru Island. Journal of Geophysical Research 103, 24641–24650.

Guilderson, T.P., Schrag, D.P., Goddard, E., Kashgarian, M., Wellington, G.M., Linsley, B.K., 2000. Southwest subtropical Pacific surface radiocarbon in a high-resolution coral record. Radiocarbon 42, 249–256.

Guilderson, T.P., Schrag, D.P., Cane, M.A., 2004. Surface water mixing in the Solomon Sea as documented by a high-resolution coral ^{14}C record. Journal of Climate 17, 1147–1157.

Gupta, S.K., Polach, H.A., 1985. Radiocarbon Dating. Radiocarbon Laboratory, Research School of Pacific Studies, Australian National University, Canberra.

Haberle, S.G., Hope, G.S., van der Kaars, S., 2001. Biomass burning in Indonesia and Papua New Guinea: natural and human induced fire events in the fossil record. Palaeogeography, Palaeoclimatology, Palaeoecology 171, 259–268.

Hénin, C., du Penhoat, Y., Ioualalen, M., 1998. Observations of sea surface salinity in the western Pacific fresh pool: large-scale changes in 1992–1995. Journal of Geophysical Research 103, 7523–7536.

Hua, Q., Jacobsen, G.E., Zoppi, U., Lawson, E.M., Williams, A.A., Smith, A.M., McGann, M.J., 2001. Progress in radiocarbon target preparation at the ANTARES AMS Centre. Radiocarbon 43, 275–282.

Hughen, K.A., Baillie, M.G.L., Bard, E., Beck, J.W., Bertrand, C.J.H., Blackwell, P.G., Buck, C.E., Burr, G.S., Cutler, K.B., Damon, P.E., Edwards, R.L., Fairbanks, R.G., Friedrich, M., Guilderson, T.P., Kromer, B., McCormac, G., Manning, S., Bronk Ramsey, C., Reimer, P.J., Reimer, R.W., Remmele, S., Southon, J.R., Stuiver, M., Talamo, S., Taylor, F.W., van der Plicht, J., Weyhenmeyer, C.E., 2004. Marine04 marine radiocarbon age calibration, 0–26 cal kyr BP. Radiocarbon 46, 1059–1086.

Koutavas, A., Lynch-Stieglitz, J., Marchitto Jr., T.M., Sachs, J.P., 2002. El Niño-like pattern in Ice Age tropical Pacific sea surface temperature. Science 297, 226–230.

Kuroda, Y., 2000. Variability of currents off the northern coast of New Guinea. Journal of Oceanography 56, 103–116.

Levitus, S., Boyer, T.P., 1994. World Ocean Atlas 1994, vol. 4: Temperature. NOAA Atlas NESDIS, Department of Commerce, Washington, DC.

Lindstrom, E., Lukas, R., Fine, R.A., Firing, E., Godfrey, S., Meyers, G., Tsuchiya, M., 1987. The western equatorial Pacific Ocean circulation study. Nature 330, 533–537.

Liu, Z., Kutzbach, J., Wu, L., 2000. Modeling climate shift of El Nino variability in the Holocene. Geophysical Research Letters 27, 2265–2268.

McAlpine, J.R., Keig, G., Falls, R., 1983. Climate of Papua New Guinea. Australian National University Press, Canberra.

McCulloch, M.T., Mortimer, G. Applications of the ^{238}U–^{230}Th decay series to dating of fossil and modern corals using MC-ICPMS. Australian Journal of Earth Sciences, in press.

McGregor, H.V., 2003. Coral reconstructions of mid-Holocene ocean–atmosphere variability in the Western Pacific Warm Pool. PhD Thesis, Research School of Earth Sciences, Aust. Nat. Univ., Canberra, p. 151.

McGregor, H.V., Gagan, M.K., 2003. Diagenesis and geochemistry of *Porites* corals from Papua New Guinea: implications for paleoclimate reconstruction. Geochimica et Cosmochimica Acta 67, 2147–2156.

McGregor, H.V., Gagan, M.K., 2004. Western Pacific coral $\delta^{18}O$ records of anomalous Holocene variability in the El Niño–Southern Oscillation. Geophysical Research Letters 31, L11204.

Moy, C.M., Seltzer, G.O., Rodbell, D.T., Anderson, D.M., 2002. Variability of El Niño/Southern Oscillation activity at millennial timescales during the Holocene epoch. Nature 420, 162–165.

Palmer, T.N., Mansfield, D.A., 1984. Response of two atmospheric general circulation models to sea surface temperature anomolies in the tropical east and west Pacific. Nature 310, 483–485.

Paterne, M., Ayliffe, L.K., Arnold, M., Cabioch, G., Tisnérat-Laborde, N., Hatté, C., Douville, E., Bard, E., 2004. Paired ^{14}C and $^{230}Th/U$ dating of surface corals from the Marquesas and Vanuatu (sub-equatorial Pacific) in the 3000 to 15,000 cal yr interval. Radiocarbon 46, 551–566.

Petchey, F., Phelan, M., White, J.P., 2004. New ΔR values for the southwest Pacific Ocean. Radiocarbon 46, 1005–1014.

Reimer, P.J., Reimer, R.W., 2001. A marine reservoir correction database and on-line interface. Radiocarbon 43, 461–463.

Reimer, P.J., Baillie, M.G.L., Bard, E., Bayliss, A., Beck, J.W., Bertrand, C.J.H., Blackwell, P.G., Buck, C.E., Burr, G.S., Cutler, K.B., Damon, P.E., Edwards, R.L., Fairbanks, R.G., Friedrich, M., Guilderson, T.P., Hogg, A.G., Hughen, K.A., Kromer, B., McCormac, G., Manning, S., Bronk Ramsey, C., Reimer, R.W., Remmele, S., Southon, J.R., Stuiver, M., Talamo, S., Taylor, F.W., van der Plicht, J., Weyhenmeyer, C.E., 2004. IntCal04 atmospheric radiocarbon age calibration, 0–26 cal kyr BP. Radiocarbon 46, 1029–1058.

Reverdin, G., Frankignoul, C., Kestenare, E., McPhaden, M.J., 1994. Seasonal variability in the surface currents of the equatorial Pacific. Journal of Geophysical Research 99, 20323–20344 doi: 0148-0227/94/94JC-01477.

Rhodes, E.G., Polach, H.A., Thom, B.G., Wilson, S.R., 1980. Age structure of Holocene coastal sediments: Gulf of Carpentaria, Australia. Radiocarbon 22, 718–727.

Rodbell, D.T., Seltzer, G.O., Anderson, D.M., Abbott, M.B., Enfield, D.B., Newman, J.H., 1999. An ~15,000-year record of El Niño-driven alluviation in southwestern Ecuador. Science 283, 516–520.

Siani, G., Paterne, M., Michel, E., Sulpizio, R., Sbrana, A., Arnold, M., Haddad, G., 2001. Mediterranean sea surface radiocarbon reservoir age changes since the Last Glacial Maximum. Science 294, 1917–1920.

Sikes, E.L., Samson, C.R., Guilderson, T.P., Howard, W.R., 2000. Old radiocarbon ages in the southwest Pacific Ocean during the last glacial period and deglaciation. Nature 405, 555–559.

Southon, J.R., Oakland Rodman, A., True, D., 1995. A comparison of marine and terrestrial radiocarbon ages from northern Chile. Radiocarbon 37, 389–393.

Southon, J., Kashgarian, M., Fontugne, M., Metivier, B., Yim, W.W.-S., 2002. Marine reservoir corrections for the Indian Ocean and southeast Asia. Radiocarbon 44, 167–180.

Stein, M., Wasserburg, G.J., Aharon, P., Chen, J.H., Zhu, Z.R., Bloom, A., Chappell, J., 1993. TIMS U-series dating and stable isotopes of the last interglacial event in Papua New Guinea. Geochimica et Cosmochimica Acta 57, 2241–2554.

Stirling, C.H., Esat, T.M., McCulloch, M.T., Lambeck, K., 1995. High-precision U-series dating of corals from Western Australia and implications for the timing and duration of the Last Interglacial. Earth and Planetary Science Letters 135, 115–130.

Stott, L.D., Cannariato, K., Thunell, R., Haug, G.H., Koutavas, A., Lund, S., 2004. Decline of surface temperature and salinity in the western tropical Pacific Ocean in the Holocene epoch. Nature 431, 56–59.

Stuiver, M., Braziunas, T.F., 1993. Modeling atmospheric ^{14}C influences and ^{14}C ages of marine samples to 10,000 BC. Radiocarbon 35, 137–189.

Stuiver, M., Polach, H.A., 1977. Discussion: reporting of ^{14}C Data. Radiocarbon 19, 355–363.

Stuiver, M., Reimer, P.J., Reimer, R.W., 2005. CALIB 5.0 [WWW program and documentation]. 〈http://radiocarbon.pa.qub.ac.uk/calib/〉.

Swadling, P., Chappell, J., Francis, G., Araho, N., Ivuyo, B., 1989. A Late Quaternary inland sea and early pottery in Papua New Guinea. Archaeology in Oceania 24, 106–109.

Tourre, Y.M., White, W.B., 1997. Evolution of the ENSO signal over the Indo-Pacific domain. Journal of Physical Oceanography 27, 683–696.

Tsuchiya, M., Lukas, R., Fine, R.A., Firing, E., Lindstrom, E., 1989. Source waters of the Pacific Equatorial Undercurrent. Progress in Oceanography 23, 101–147.

Tudhope, A.W., Chilcott, C.P., McCulloch, M.T., Cook, E.R., Chappell, J., Ellam, R.M., Lea, D.W., Lough, J.M., Shimmield, G.B., 2001. Variability in the El Niño–Southern Oscillation through a glacial–interglacial cycle. Science 291, 1511–1517.

Yan, X., Ho, C., Zheng, Q., Klemas, V., 1992. Temperature and size variabilities of the Western Pacific Warm Pool. Science 258, 1643–1645.